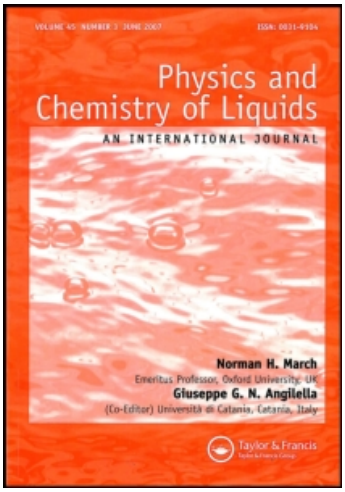

Physics and Chemistry of Liquids
Publication details, including instructions for authors and subscription information:
http://www.informaworld.com/smpp/title~content=t713646857

Influence of temperature-induced liquid-liquid structure transition on directional solidification microstructure of Sn-Bi40wt-% alloy

L. J. Liu[a]; M. Q. Liu[a]; F. Q. Zu[a]; Z. Y. Huang[a]; C. M. Hu[a]; L. N. Mao[a]
[a] Liquid/Solid Metal Processing Institute, School of Materials Science & Engineering, Hefei University of Technology, Hefei 230009, P.R. China

Online publication date: 03 June 2010

To cite this Article Liu, L. J. , Liu, M. Q. , Zu, F. Q. , Huang, Z. Y. , Hu, C. M. and Mao, L. N.(2010) 'Influence of temperature-induced liquid-liquid structure transition on directional solidification microstructure of Sn-Bi40wt-% alloy', Physics and Chemistry of Liquids, 48: 3, 329 — 336
To link to this Article: DOI: 10.1080/00319100902839152
URL: http://dx.doi.org/10.1080/00319100902839152

Physics and Chemistry of Liquids
Vol. 48, No. 3, June 2010, 329–336

Taylor & Francis
Taylor & Francis Group

Influence of temperature-induced liquid–liquid structure transition on directional solidification microstructure of Sn–Bi40wt-% alloy

L.J. Liu*, M.Q. Liu, F.Q. Zu, Z.Y. Huang, C.M. Hu and L.N. Mao

Liquid/Solid Metal Processing Institute, School of Materials Science & Engineering, Hefei University of Technology, Hefei 230009, P.R. China

(*Received 11 January 2009; final version received 22 February 2009*)

Prior investigation suggested that a temperature-induced liquid–liquid structure transition (TI-LLST) could occur in Sn–Bi40wt-% alloy around 879°C. Based on the results of TI-LLST, the Sn–Bi40wt-% alloys are melted and held at the temperature above and below TI-LLST, respectively, and then solidified from the same temperature. The aim of this work was to explore the influence of TI-LLST on directional solidification microstructure by using the Bridgman method. The results show that dendritic arm spacing decreases and the microstructure is refined markedly for the samples solidified from the melt which experienced the TI-LLST.

Keywords: TI-LLST; Sn–Bi40wt-%; directional solidification; dendritic arm spacing; directional solidification microstructure

1. Introduction

It is well accepted that the structure of liquids has direct influences on the microstructure and properties of materials [1]. The structure of liquids is playing an increasingly important role in the manufacture of high-quality metallic materials. Fortunately, the explorations of liquid structures have made many exciting achievements in recent years. However, the different solidification structure is often owed to the difference of the melt's structure, and the essence of the effect needs to be studied further.

Liquid–liquid structure transition (L-LST) has been observed in some binary alloys, such as In–Sn, In–Bi, Pb–Sn, Pb–Bi and Sn–Bi. It has been established that the liquid structure transition occurs at certain temperature range in Sn–Bi alloys with different compositions by using DC four probe method [2]. Furthermore, the solidification microstructures of Al–Si [3] and Bi–Sb [4] were changed remarkably after the melt experienced the temperature-induced liquid–liquid structure transition (TI-LLST). It has been accepted that the temperature can induce the L-LST, but its effects on directional solidification microstructure have not been investigated. Therefore, there is a strong interest in determining the effects of TI-LLST on directional solidification microstructure.

*Corresponding author. Email: lmq5012@hotmail.com

ISSN 0031–9104 print/ISSN 1029–0451 online

DOI: 10.1080/00319100902839152
http://www.informaworld.com

One of the main techniques used in directional solidification is the Bridgman technique, which allows the thermal gradient at the interface and the solidification rate to be imposed independently. Directional solidification techniques enable the solidification structure of materials to be put in order along a specific direction, namely as a directional or single crystal structure, which could improve the mechanical and physical properties of materials [5–8]. For high-quality materials, metallurgists and the materials engineers need to know more about how to control the solidification process so as to create desired microstructures on demand. In spite of many developments in directional solidification, this is a huge field that needs constant investigations.

The Sn–Bi alloys have received much attention because of their good properties as solders for some delicate electronic tools [9]. In this article, directional solidification studies have been carried out to investigate the changes of the directional solidification microstructures, with the same temperature gradient, G, and solidification rate, V. With Bi being segregated there is no thermosolutal convection. The main purpose of this article is to explore the influence of TI–LLST on directional solidification microstructure of Sn–Bi40wt-% alloy. Further, the relation between the TI-LLST and directional solidification microstructure was discussed through the results of solidification experiments.

2. Experimental details

All samples were prepared from high-purity Sn (5 N) and Bi (5 N). As seen in Figure 1, the resistivity–temperature (ρ–T) curves of the melt change abnormally. Moreover, the changing pattern in the first heating process is completely different from the ones in the subsequent heating and cooling cycles. Since resistivity is a structural sensitive parameter, these abnormal changes of ρ–T curves indicate that TI-LLST probably occur in Sn–Bi40wt-% melt, with some reversible characters. Based on the TI-LLST, 600°C (below TI-LLST temperature) and 1000°C (above TI-LLST temperature), were selected as holding temperature. Each sample, which weighed 20 g, was melted in alundum crucible. All samples were covered with B_2O_3 slag to prevent them from evaporation and oxidation during the entire melting process. Sample A was heated to 600°C and held for an hour in an electrical resistance furnace, the melt was poured into the 12-cm long × 6-mm-i.d. quartz tube for the unidirectional solidification experiments. Sample B was first heated to 1000°C and held for half an hour. Second, it was transported into another electrical resistance furnace, which had been heated to 600°C, held for half an hour. Third, the melt was also poured into the 12-cm long × 6-mm-i.d. quartz tube for the unidirectional solidification experiments. The melt preparation procedure is shown in Table 1. All the melt would hold at the same temperature of 600°C before solidification in order to eliminate the effects of sensible heat.

In the unidirectional solidification apparatus used in this study, the sample tube remains stationary and the temperature gradient is set up at the temperature between the furnace and a cooling chamber. The furnace is moved upward by the drive mechanism at the desired velocity.

During the unidirectional solidification experiments, the temperature gradient was controlled by the temperature of the furnace because the cooling chamber

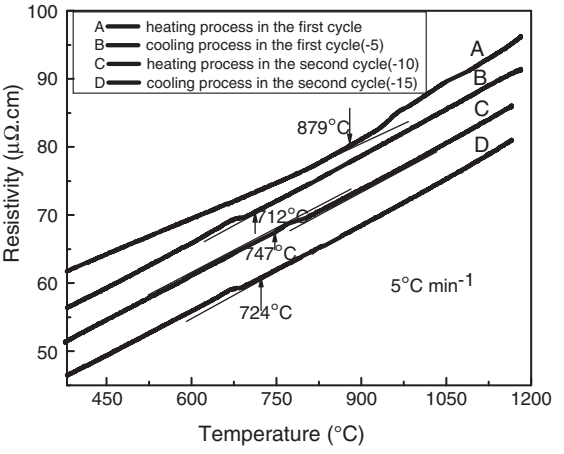

Figure 1. Resistivity–temperature curves of Sn–Bi40wt-%.

Table 1. Melts preparing procedure and solidification medium for Sn–Bi40wt-% alloy.

Melting temperature and holding time before solidification	
Sample A	600°C, 1 h
Sample B	1000°C, 0.5 h + 600°C, 0.5 h

temperature remained relatively constant. The temperature of the furnace was maintained at 400°C. Unidirectional solidification was carried out at the chosen rate ($100\,\mu m\,s^{-1}$) until the desire fraction of the sample was solidified, the time at which the sample was quenched to preserve the interface structure. Microstructures of the specimens were investigated by an optical microscope and dendritic arm spacing were measured on the transverse section by a Quantimet 500 image analysis system. The number of primary dendritic arm spacingn in a known area A was counted and the primary dendritiiz arm spacing was calculated as $\lambda_1 = (A/n)^{0.5}$. The second dendritic arm spacing was measured on the longitudinal section within the mushy zone.

3. Results

In these experiments, the microstructure on longitudinal section of samples was examined for Sn–Bi40wt-% alloy. L is the distance between the observed position and the bottom of the sample. Figures 2–4 show, respectively, the microstructure on longitudinal section of samples at $G = 10\,K\,mm^{-1}$, $V = 100\,\mu m\,s^{-1}$ and $L = 5$, 10 and 15 mm. Corresponding to the TI-LLST, there is a great transformation of the directional solidification microstructures for samples A and B. By comparing them, it can be observed distinctly that either the primary phase or the eutectic phase of sample B is evidently finer than that of sample A.

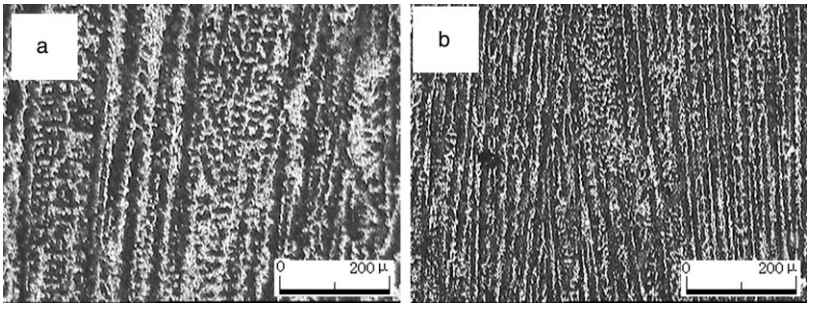

Figure 2. The microstructure on longitudinal section of samples for Sn–Bi40wt-% alloy at $G = 10\,\mathrm{K\,mm^{-1}}$, $V = 100\,\mu\mathrm{m\,s^{-1}}$ and $L = 5\,\mathrm{mm}$; (a) sample A and (b) sample B.

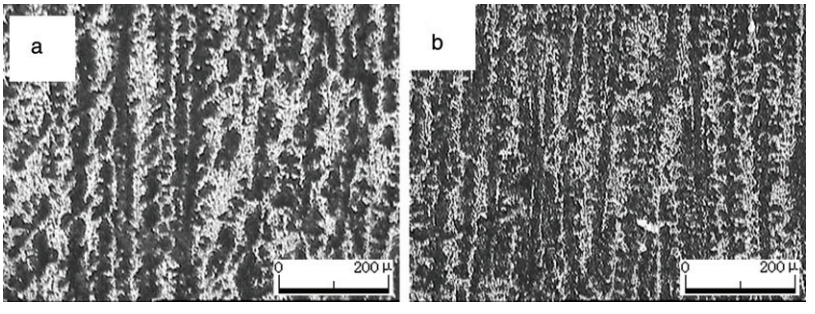

Figure 3. The microstructure on longitudinal section of samples for Sn–Bi40wt-% alloy at $G = 10\,\mathrm{K\,mm^{-1}}$, $V = 100\,\mu\mathrm{m\,s^{-1}}$ and $L = 10\,\mathrm{mm}$; (a) sample A and (b) sample B.

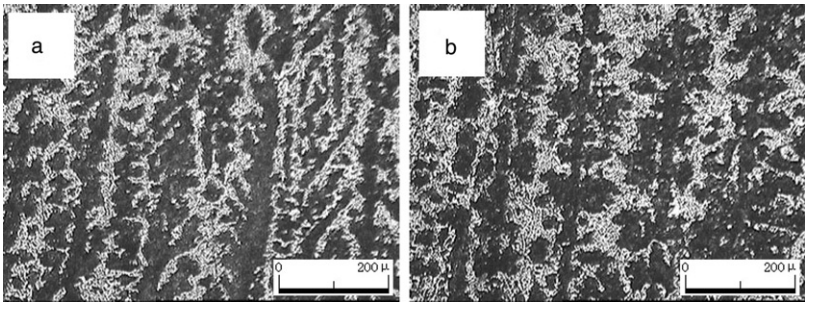

Figure 4. The microstructure on longitudinal section of samples for Sn–Bi40wt-% alloy at $G = 10\,\mathrm{K\,mm^{-1}}$, $V = 100\,\mu\mathrm{m\,s^{-1}}$ and $L = 15\,\mathrm{mm}$; (a) samples A and (b) B.

Figure 5 shows the dendritic structure on the transverse section of Sn–Bi40wt-% alloy. It can be seen that dendritic arm spacing were greatly refined for the sample solidified from the melt experienced the TI-LLST. The primary dendritic arm spacing λ_1 can be produced to be 80 μm, just 4/5 as that of sample A, which was not solidified from the melt experienced the TI-LLST.

Figure 6 shows the quenched liquid/solid interfaces in Sn–Bi40 wt-% samples. It can be observed distinctly that the second dendrite arm spacing in the mushy zone was greatly refined for the sample B, which was solidified from the melt experienced the TI-LLST.

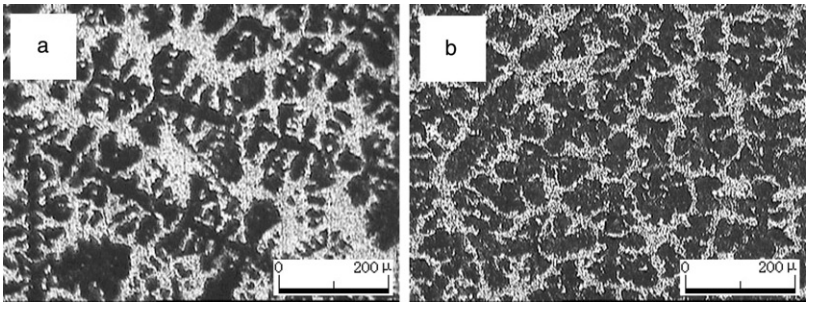

Figure 5. The microstructure on cross-section of samples for Sn–Bi40wt-% alloy at $G = 10\,\mathrm{K\,mm^{-1}}$, $V = 100\,\mu\mathrm{m\,s^{-1}}$ and $L = 10\,\mathrm{mm}$; (a) samples A and (b) B.

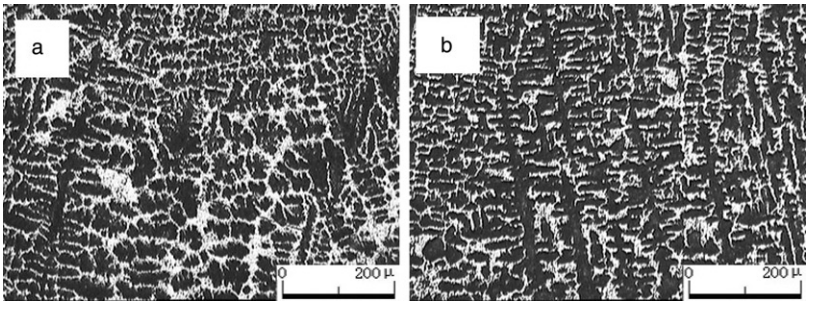

Figure 6. The microstructure on longitudinal section of samples for Sn–Bi40wt-% alloy at $G = 10\,\mathrm{K\,mm^{-1}}$ and $V = 100\,\mu\mathrm{m\,s^{-1}}$; (a) sample A and (b) sample B.

4. Discussion

For liquid Sn–Bi40wt-% alloy, there are probably some metastable Sn- and Bi-rich clusters in the melt at a low temperature above the liquidus temperature [10]. With the temperature further rising, these metastable clusters are broken until the melt reach a stable state, at the same time, new liquid structure build up. This metastable to stable transition in liquid Sn–Bi40wt-% alloy is irreversible.

The neutron scattering experiment of liquid Sn shows that there is a clear shoulder on the high-Q side of the first peak of $S(Q)$ at 846 and 1046°C, and even at 2146°C, such a shoulder may still be present [11]. Based on the result of neutron scattering experiment, the stable liquid Sn–Bi40wt-% alloy include some tetrahedral short range orders with reversible characters, i.e. they can reassemble at the TI-LLST temperature on cooling and break at the TI-LLST temperature on heating.

For liquid Sn–Bi40wt-% alloy, the melt mainly consists of Sn- and Bi-rich clusters below TI-LLST temperature. When the heating temperature is up to the critical temperature, the energy of the atoms becomes high enough to overcome the energy barrier so that the Sn–Sn or Bi–Bi atomic bonds in melt are continuously broken and the new Sn–Bi atomic bonds come into being. Meanwhile, the melt becomes more homogeneous and disordered.

After the Sn–Bi40wt-% alloy is melted, there is a mass of atomic clusters similar to the corresponding solid in the melt. When the melt is hold at 600°C, these atomic clusters still exist. By the fluctuation of structure and energy, those clusters can easily extend to the critical size of crystal nucleus under a low undercooling. In this case it is convenient for the primary phase to nucleate, so that the primary phase can easily grow to larger size.

When the melt is heated to a relative high temperature above TI-LLST temperature, the atomic clusters similar to the corresponding solid will break up and the melt will become more uniform and disordered. According to the classical nucleation theory [12], the smaller and disordered clusters cannot grow to the size of critical size of nucleation unless under a greater undercooling.

Especially, the difference between samples A and B should not be attributed to impurities in the liquid phase which are derived from the reactions with the B_2O_3 used or the crucible material. In the exploration of the universality of TI-LLST, the abnormal changes of the electrical resistivity are not observed in some liquid, e.g. Bi–Zn and some compositions of Sn–Sb [13]. In those experiments, the B_2O_3 and the same crucible material were all used. In addition, the microstructure of Sn–Sb42wt-% alloy has no obvious change at the same pouring temperature, but the highest temperatures of thermal treatment are different. These phenomena indicate that the TI-LLST do occur with temperature rising and the marked difference between samples A and B should not be credited to the reactions with the B_2O_3 used or the crucible material.

Some analytical models of the dependence of primary dendritic arm spacing on the solidification parameters (thermal gradient G_1 and the solidification rate V) in binary alloy have been proposed [14]. Hunt gave the following relationship for:

$$\lambda_1 = AG_1^{-0.5}V^{-0.25}. \tag{1}$$

The secondary dendritic arm spacing λ_2 predicted by the analytical model is described as:

$$\lambda_2 = B(G_1V)^{-1/3} \tag{2}$$

where A and B are constants dependent on the composition of the alloy. With the increase of solidification rate, dendritic arm spacing can be greatly refined. But the directional solidification experiments in this article have been carried out at the chosen rate ($100\,\mu m\,s^{-1}$), the decrease of primary dendritic arm spacing for sample B can be attributed to influence of TI-LLST. If the sample is solidified from the melt which experienced the TI-LLST, superfine dendritic structure can be obtained.

In the heating process, TI-LLST occurs and changes the free energy of melt system. Then it affects the growth rate of the crystal nucleus. An energy model is introduced (Figure 7) to show the changes of free energy of melt system caused by TI-LLST. ΔG_m is the free energy change between liquid and solid. ΔG_b is the energy barrier a atom had to overcome from liquid to solid before TI-LLST. $\Delta G_{b'}$ is the decrease of free energy of liquid caused by TI-LLST. Though the TI-LLST of Sn–Bi40wt-% is partly reversible, the free energy of the melt will still keep at a relatively lower state before solidification occurs.

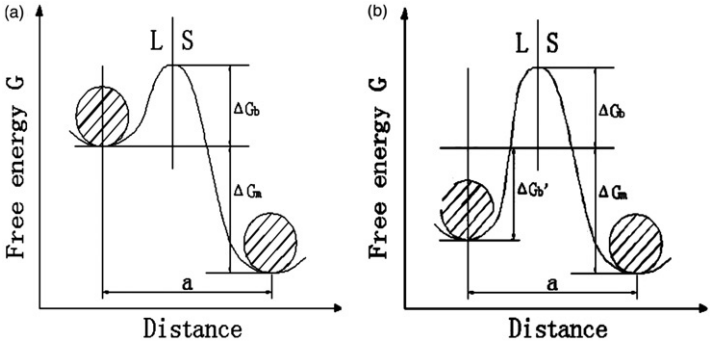

Figure 7. Sketch of Gibbs free energy in liquid–solid interface: ΔG_b, the energy barrier to overcome for liquid-to-solid transfer of melt clusters before TI-LLST, $\Delta G_{b'}$, for the melt having experienced TI-LLST, an additional energy barrier to overcome for resetting atoms from the distinct arrangement of the clusters to lattice sites of the growing crystal after the initial attachment and $\Delta G_m + \Delta G_b$, the energy barrier to overcome for solid-to-liquid transfer of melt clusters. (a) Before TI-LLST; (b) after TI-LLST.

If the alloys are melted below the TI-LLST temperature, the transfer frequencies that an atom jumps the energy barrier of liquid to solid and solid to liquid can be described by

$$v_{LS} = v_0 \exp[-\Delta G_b/KT] \tag{3}$$

$$v_{SL} = v_0 \exp[-(\Delta G_b + \Delta G_m)/KT] \tag{4}$$

where v_0 is the vibrational frequency of an atom and K is the Boltzmann's constant. And the net transfer frequency is

$$v_{\text{net}} = v_{LS} - v_{SL} = v_0 \exp(-\Delta G_b/KT)[1 - \exp(-\Delta G_m/KT)]. \tag{5}$$

While the alloys are melted above the TI-LLST temperature, the net transfer frequency is

$$v'_{\text{net}} = v_0 \exp[-(\Delta G_b + \Delta G_{b'})/KT] \cdot [1 - \exp(-\Delta G_m/KT)]. \tag{6}$$

Deduced from $R = a v_{\text{net}}$ (a is a constant for definite matter), we attain that $R' < R$ because $v'_{\text{net}} < v_{\text{net}}$. As shown in Figure 6, the free energy of the melt system decreases by ΔG_b after TI-LLST, the growth rate R' of crystal nucleus after TI-LLST is smaller than R before TI-LLST in solidification process, which finally decreases the size of primary phase.

5. Conclusions

The marked change of morphology of Sn–Bi40wt-% alloy solidified from the same temperature in the same conditions is due to the debonding of the atomic clusters similar to the corresponding solid. The microstructure is refined markedly for the

sample solidified from the melt which experienced the TI-LLST. The primary dendritic arm spacing λ_1 can be produced to be 80 μm, just as 4/5 as that of sample A, which was not solidified from the melt experienced the TI-LLST.

The results of experiments indicate that TI-LLST has great effects on solidification behaviour and solidified structures. So, this finding is meaningful for the study of the micro-mechanism of solidification, and is helpful for improving the solidified morphology and mechanical properties.

Acknowledgements

This work is financially supported by the National Natural Science Foundation of China, Grant No. 50571033, and the Provincial Natural Science Foundation of Anhui, China, Grant Nos. 070416234 and 070414178. The authors would like to give their thanks to two anonymous reviewers for their helpful suggestions for improving this article.

References

[1] F. Sette and M.H. Krisch, J. Sci. **280**, 1550 (1998).
[2] X.F. Li, F.Q. Zu, and H.F. Ding, J. Phys. Lett. A **354**, 325 (2006).
[3] O. Tatsuya and K.J. Masayuki, J. Jpn Inst. Met. **58**, 1311 (1994).
[4] X.F. Li, F.Q. Zu, J. Yu, and B. Zhou, J. Phase Transit. **81**, 43 (2008).
[5] H.Z. Fu, presented at the First Pacific Rim International Conference on Advanced Materials and Processing, 1992 (unpublished).
[6] G.J.S. Higginborham, J. Mat. Sci. Technol. **2**, 442 (1986).
[7] S. Yang, W.D. Huang, X. Lin, and Y.H. Zhou, J. Ordnance Mat. Sci. Eng. **23**, 44 (2000).
[8] Z.P. Zhou and R.D. Li, J. Special Casting Nonferrous Alloys **20**, 35 (2003).
[9] K.S. Dogra, Int. Electronics Packaging 90c (Glen Ellyn, IL, USA, 1986).
[10] H. Aoki, K. Hotoduka, and T. Itami, J. Non-Cryst Solids **312–314**, 222 (2002).
[11] J.P.P. Gaspard, C. Lambin, and J.P. Vigneron, J. Phil. Mag. B **50**, 10 (1984).
[12] H.Q. Hu, *The Principle of Metal Solidification* (Machine Press, Beijing, 2000).
[13] F.Q. Zu, R.R. Shen, and Y. Xi, J. Phys.: Condens. Matter. **18**, 2817 (2006).
[14] H.Q. Hu, *Fundamental of Metal Solidification* (Mechanical Industry Publishing, Beijing, 1991).